

Pressure-induced metal-insulator transition in LaMnO_3 is not of Mott-Hubbard type

A. Yamasaki, M. Feldbacher, Y.-F. Yang, O. K. Andersen, and K. Held
Max-Planck Institut für Festkörperforschung, D-70569 Stuttgart, Germany
 (Dated: July 18, 2018)

Calculations employing the local density approximation combined with static and dynamical mean-field theories (LDA+ U and LDA+DMFT) indicate that the metal-insulator transition observed at 32 GPa in paramagnetic LaMnO_3 at room temperature is not a Mott-Hubbard transition, but is caused by orbital splitting of the majority-spin e_g bands. For LaMnO_3 to be insulating at pressures below 32 GPa, both on-site Coulomb repulsion and Jahn-Teller distortion are needed.

PACS numbers: 71.30.+h 71.20.-b 71.27.+a

Since the discovery of colossal magnetoresistance (CMR) [1], manganites have been intensively studied. The key to understand CMR is the high-temperature paramagnetic insulating-like phase, which is characterized not only by an increase of resistivity with decreasing temperature, but also by unusual dynamical properties, such as low spectral weight at the Fermi level for a wide range of doping [2, 3, 4]. Theoretical understanding of this hole-doped paramagnetic phase remains incomplete, and CMR transition temperatures are lower than technologically desirable.

In this Letter, we shall focus on the pressure-induced insulator-metal (IM) transition in the undoped parent compound LaMnO_3 with configuration $t_{2g}^3 e_g$. This transition occurs at room temperature, well above the magnetic ordering temperature ($T_N=140$ K), well below the cooperative Jahn-Teller (JT) temperature ($T_{oo}=740$ K at 0 GPa), and at a hydrostatic pressure of 32 GPa where the JT distortion appears to be completely suppressed [5]. The IM transition thus seems to be a bandwidth-driven Mott-Hubbard transition of the e_g electrons and points to the dominating importance of the Coulomb repulsion between two e_g electrons on the same site. This is supported by recent self-interaction-corrected local density approximation (LDA) calculations, performed, however, for the cubic structure and magnetically ordered states at low temperature [6]. Structural distortions at 0 K as functions of pressure were recently calculated with the LDA+ U method [7]. On the theoretical side, it has been an issue of long debate whether the JT distortion or the Coulomb repulsion is responsible for the insulating behavior of LaMnO_3 at normal pressure. The high-pressure experiment [5] seems to favor the latter.

Here, we shall study the room-temperature electronic structure of LaMnO_3 at normal pressure and the pressure-induced IM transition by means of LDA + U [8] and LDA + dynamical mean field theory (DMFT) [9] calculations. Upon going from the insulating to the metallic, high-pressure phase, we shall find that the orbital polarization and the concomitant splitting of the two majority-spin e_g bands are gradually reduced. The IM transition takes place when the bands start to overlap. Since this occurs within the (orbitally) symmetry-broken

phase, this IM transition is not a Mott-Hubbard transition. The Coulomb interaction, *as well as* the JT distortion are needed for a proper description of this transition and the insulating nature of LaMnO_3 .

The orthorhombic crystal structure of LaMnO_3 at atmospheric pressure is shown in Fig. 1. The O_6 octahedra are elongated in the y direction (nearly parallel to $\mathbf{b}-\mathbf{a}$ in Fig. 1) in subcells 1 and 3, and in the x direction (nearly parallel to $\mathbf{b}+\mathbf{a}$) in subcells 2 and 4. This JT distortion decreases linearly from 11% at 0 GPa, to 4% at 11 GPa, the highest pressure for which internal parameters were measured [5]. The GdFeO_3 -type distortion tilts the corner sharing octahedra around the b axis and rotates them around the c axis, both in alternating directions. When the pressure increases from 0 to 11 GPa, the tilt is reduced from 12° to 8° and the rotation from 7° to 5° .

The top right-hand side of Fig. 2 shows the paramagnetic LDA bands at normal pressure and the left-hand side those for a hypothetical, cubic structure with the same volume. The dashed blue bands were obtained with a large basis set of N th-order muffin tin orbitals (NMTOs) [10, 11]. Within the frame of the figure, we see the $3(\times 4)$ Mn t_{2g} and the $2(\times 4)$ Mn e_g bands, while the O $2p$ bands are below. As a check, we also carried

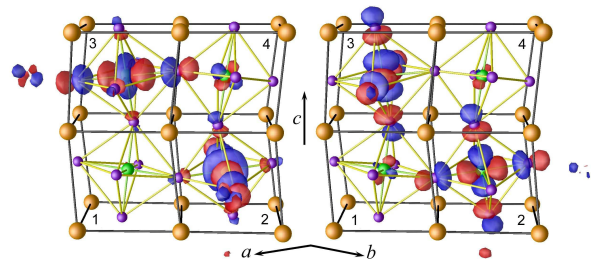


FIG. 1: (color). LaMnO_3 orthorhombic translational cell ($Pbnm$) and LDA-NMTO Mn e_g crystal-field orbitals |1> (left) and |2> (right) of, respectively, lowest and highest energy. For the sake of clarity, the orbitals have been placed only in subcells 3 and 2; those in subcells 1 and 4 may be obtained by the LaO mirror plane perpendicular to the c ($=z$) axis. Since they have antibonding O $2p$ tails, orbitals |1> and |2> are directed, respectively, along and perpendicular to the longest Mn-O bond. Red/blue indicates a positive/negative sign.

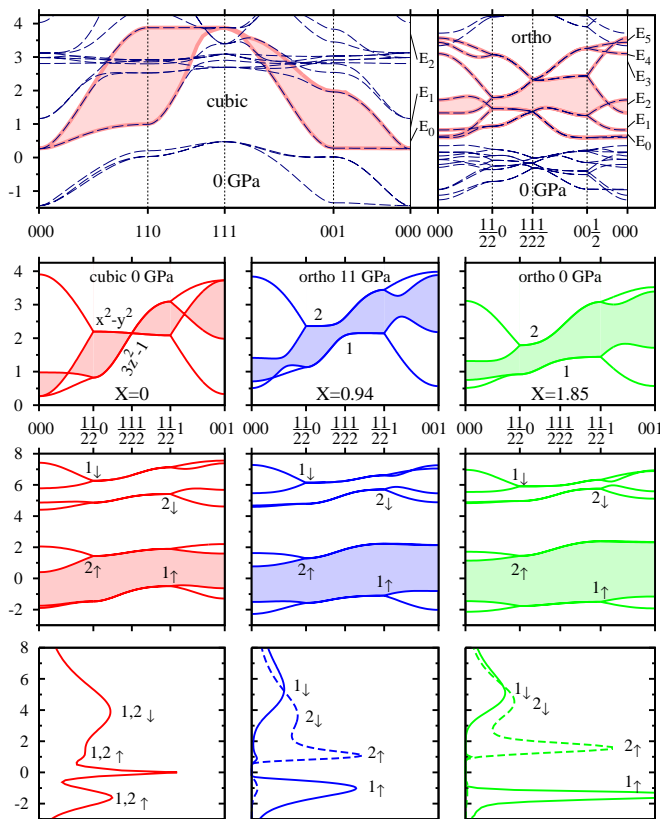


FIG. 2: (color). *Top*: Paramagnetic LDA band structure for orthorhombic (right) and hypothetical cubic (left) LaMnO_3 at 0 GPa plotted along the high-symmetry lines in the $k_x=k_y$ plane. Energies are in eV, the \mathbf{k} unit is π [11], and the \mathbf{k} points marked are $\Gamma\text{MRX}\Gamma$ in the cubic, and $\Gamma\text{YTZ}\Gamma$ in the orthorhombic BZ. The latter is folded in from the former and has the following smallest inequivalent reciprocal-lattice vectors: $\mathbf{Q} = 000, 110, 111,$ and 001 . Dashed blue bands: large NMTO basis set; red bands: Mn e_g NMTO basis set employed in Eq. (1). The $N+1$ support energies E_i are shown at the right-hand sides. The zero of energy corresponds to configuration t_{2g}^4 . *Second row*: 0 and 11 GPa orthorhombic (0 GPa cubic) e_g bands folded out (in) to the $(000, 110)$ -BZ. The dimensionless band-shape parameter, X , is the LDA crystal-field splitting in units of the effective hopping integral $t \equiv |t_{dd\sigma}| \sim W/6$, both obtained from the NMTO Mn e_g Wannier functions. *Third row*: As second row, but obtained by spin-polarized LDA+ U for random spin orientations (room temperature). Bands are labelled by their main character. The zero of energy is the Fermi level. *Bottom*: Spectra calculated by LDA+DMFT. The full and dashed lines give the projections onto orbitals |1) and |2), respectively.

out spin-polarized calculations for ferro- and antiferromagnetic A -type orders and found full agreement with previous work [12]. Near the top of Fig. 2 —and continuing above it— is the La $5d$ band which is pushed 2 eV up by $pd\sigma$ hybridization with oxygen when going from the cubic to the orthorhombic structure. This hybridization is a reason for the GdFeO_3 -type distortion [11], but since it only involves $O p$ orbitals perpendicular to the

one which hybridizes with Mn e_g (Fig. 1), the La $5d$ and Mn e_g bands hardly hybridize. Finally, the narrow band crossing the cubic Mn e_g band is La $4f$.

The NMTO method can be used to generate minimal basis sets [10, 11], such as the Mn e_g basis whose orbitals are shown in Fig. 1. This basis gives rise to the red solid bands in the topmost panel of Fig. 2, which are seen to follow the blue dashed bands exactly, except where the latter have avoided crossings with La bands. When their energy mesh is converged, the symmetrically orthonormalized, minimal NMTO set is a set of Wannier functions. The e_g NMTOs are localized by the requirement that a Mn e_g orbital has *no* e_g character on neighboring Mn atoms, and this confines the NMTO-Wannier functions to being essentially as localized as those in [13].

Taking the Coulomb repulsion and Hund's exchange into account, three electrons localize in the t_{2g} orbitals which we describe in the following by a classical spin S . These t_{2g} spins, which we assume to have random orientations at room temperature, couple to the e_g electrons with strength $2\mathcal{J}S=2.7$ eV, as estimated by the splitting of the e_g^\uparrow and e_g^\downarrow bands in our ferromagnetic NMTO calculation (not shown). This results in the following low-energy Hamiltonian for the two e_g -bands:

$$\hat{H} = \sum_{ijm\sigma\sigma'} h_{im,jn} \hat{c}_{im\sigma}^\dagger u_{\sigma\sigma'}^{ij} \hat{c}_{jn\sigma'} - \mathcal{J}S \sum_{im} (\hat{n}_{im\uparrow} - \hat{n}_{im\downarrow}) + U \sum_{im} \hat{n}_{im\uparrow} \hat{n}_{im\downarrow} + \sum_{i\sigma\sigma'} (U' - \delta_{\sigma\sigma'} J) \hat{n}_{i1\sigma} \hat{n}_{i2\sigma'}, \quad (1)$$

where $h_{im,jn}$ is the LDA Hamiltonian in the representation of the two ($m=1,2$) e_g NMTO-Wannier orbitals per site (Fig. 1 and two top rows of Fig. 2); $u_{\sigma\sigma'}^{ij}$ accounts for the rotation of the spin quantization axis (parallel to the t_{2g} spin) from Mn sites j to i . The second line describes the Coulomb interactions between e_g electrons in the same (U) and in different orbitals (U'); J is the e_g - e_g Hund's rule exchange. We take $U=5$ eV and $J=0.75$ eV from the literature [3]; by symmetry, $U' = U - 2J$. These values are reasonable, also in comparison with those used for other transition-metal oxides. Whereas a larger U is appropriate when all five d degrees of freedom are treated [12], the smaller value used for our e_g Hamiltonian takes the screening by the t_{2g} electrons into account.

We first solve (1) by DMFT [14] using quantum Monte Carlo (QMC) simulations at room temperature. Previous calculations for LaMnO_3 with electronic correlations, but simplified hopping integrals, include Ref. [15]. We neglected the (orbital) off-diagonal elements of the on-site Green function, forcing the DMFT density to have the same symmetry as the LDA crystal field (Fig. 1), a good approximation for e_g systems.

The spectral densities calculated using the observed crystal structures at 0 and 11 GPa [5] are shown at the bottom of Fig. 2 (green and blue, respectively). At 0 GPa, we find strong orbital polarization, a 2 eV gap,

and, above 3 eV, spectral densities which correspond to e_{g1}^\downarrow and e_{g2}^\downarrow configurations antiparallel to the t_{2g} spin at that site. Experiments for undoped LaMnO_3 show similar —albeit less sharp— gaps [2, 3, 4]. At 11 GPa, we find the gap to be halved, but the orbital polarization to be just slightly reduced.

Since for higher pressures the internal structural parameters are unknown, we scaled the 11 GPa structure uniformly and calculated the LDA e_g bandwidth W as a function of compression. The result is shown in blue on the left-hand side of Fig. 3. On the right-hand side, we show the gap obtained from LDA+DMFT for various values of W (blue solid line), keeping the LDA band shape constant. We see that the gap decreases, but does not close before $W=7$ eV, which corresponds to a pressure way beyond the experimental 32 GPa.

Let us now turn to the cubic phase (red), for which LDA+DMFT yields *metallic* behavior already at 0 GPa (left-hand side of Fig. 2) [16]. The spectral density exhibits a quasiparticle peak at ε_F , lower and upper Hubbard bands at about ∓ 1.5 eV, and a peak due to the antiparallel-spin configurations around 4 eV. In the right-hand side of Fig. 3, we show how the quasiparticle weight Z decreases with volume expansion, and does not vanish before $W=2.7$ eV. One needs to *pull* the cubic crystal to make it insulating! Both types of structure, the cubic ($X=0$, red) and the one observed at 11 GPa ($X=0.94$, blue) give grossly wrong pressures for the IM transition —way beyond the expected errors of the LDA and DMFT approximations. Hence, we can conclude that the IM transition occurs at a reduced (compared to the one at

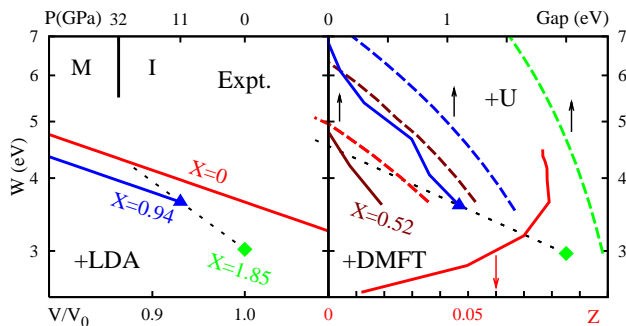


FIG. 3: (color). *Left*: LDA e_g bandwidths, $W \sim 6t$, calculated as functions of compression, V/V_0 . The top abscissa gives the experimental pressures, with 32 GPa marking the observed IM transition [5]. *Right*: 300 K LDA+DMFT (solid lines) and LDA+ U (dashed lines) results calculated as functions of W . For insulators, we plot the DOS gap (top scale) and for metals the quasiparticle weights (bottom scale). Full symbols indicate actual experimental structures and connecting black dotted lines are extrapolations. Each curve was calculated with fixed structure type (band shape): orthorhombic 0 GPa (green, $X=1.85$), orthorhombic 11 GPa (blue, $X=0.94$), cubic plus crystal-field splitting (dark red, $X=0.52$), and cubic (red, $X=0$).

11 GPa), but finite distortion [16]. Such an intermediate distortion of $X=0.52$ (dark red line) indeed yields the IM transition at roughly the correct experimental pressure as seen by using the left hand-side of Fig. 3 to translate bandwidths into pressures. A finite distortion at the IM transition is also in accord with the observed noncubic crystal structure at the IM transition [5]. Besides the JT distortion, the Coulomb interaction is absolutely essential to describe insulating LaMnO_3 . Without it, one would just obtain the metallic LDA bands shown in the second row of Fig. 2, albeit with a width reduced by $\frac{2}{3}$ due to the random spin orientation.

A detailed understanding of the band structure in the insulating phase may be obtained by treating the e_g Hamiltonian (1) in the static mean field approximation (LDA+ U) as done by Ahn and Millis [17], but using the accurate NMTO Hamiltonian. This is supported by the similarity of the resulting LDA+ U gap-versus- W curves shown by the dashed green, blue, dark red, and red lines in the right-hand side of Fig. 3 to those obtained by DMFT. The LDA+ U treatment overestimates the gaps [18], but since it is easy to follow, we use it in the remainder of this Letter to explain —almost analytically— the development of the electronic structure, starting with the cubic e_g LDA bands, then turning on the orthorhombic distortions, and finally the spin and the e_g - t_{2g} and e_g - e_g Coulomb interactions.

In the cubic structure, the two e_g bands never cross, as seen in the top left-hand side of Fig. 2. Since the dominating, indirect d_{pd} , as well as the direct dd contributions to the hopping integrals (off-site elements of $h_{im,jn}$) between nearest neighbors in the $z=0$ plane are bonding (negative), the bottom of the band is at 000 and the top at 111. In the $k_x=k_y$ plane the eigenfunctions are the $d_{3z^2-1}(\mathbf{k})$ and $d_{x^2-y^2}(\mathbf{k})$ Bloch functions, with the former band lying lower. The hopping integrals are close to those of a first-nearest-neighbor tight-binding (TB) model with $t_{dd\delta}=0$ and $t_{dd\sigma}=-t$. In this model, the cubic bandwidth is $W=6t$, and the band is symmetric around its center: $\varepsilon_2(\mathbf{k}) = -\varepsilon_1(\mathbf{k}-[111]\pi)$. In the $k_x=k_y=k$ plane, the dispersions of the d_{3z^2-1} and $d_{x^2-y^2}$ bands are, respectively, $-t \cos k - 2t \cos k_z$ and $-3t \cos k$.

In order to understand the orthorhombic bands in the top right-hand side of Fig. 2, one should first note that mirroring an e_g orbital in the LaO plane is equivalent to translating it along z . The 8 orthorhombic bands can therefore be folded *out* across the Brillouin zone (BZ) face $k_z=\frac{\pi}{2}$ to the 4 green bands shown in the second row. The blue bands were calculated for the less distorted 11 GPa structure, and the 4 red bands are the 2 cubic bands, folded *into* the $\mathbf{Q}=(110)\pi$ BZ [11]. We see that the dominating effect of the distortion is to couple the bands, and thereby to *cut* the e_g band *in two*, which overlap by *less than* W . For $k_x=k_y$, there is no coupling between $\varepsilon_{x^2-y^2}(\mathbf{k})$ and $\varepsilon_{3z^2-1}(\mathbf{k})$, but only between $\varepsilon_{3z^2-1}(\mathbf{k})$ and $\varepsilon_{x^2-y^2}(\mathbf{k}-\mathbf{Q})$. This allows us to

fold the 4 bands out to merely 2, letting not only k_z , but also $k_x=k_y\equiv k$ run from $-\pi$ to π . In the TB model, these two bands are the eigenvalues of a 2×2 matrix with diagonal elements $-t \cos k - 2t \cos k_z + (\Delta - \sqrt{3}\delta)/4$ and $3t \cos k - (\Delta - \sqrt{3}\delta)/4$ between, respectively, $d_{3z^2-1}(\mathbf{k})$ and $d_{x^2-y^2}(\mathbf{k}-\mathbf{Q})$, and with the off-diagonal element $-(\sqrt{3}\Delta + \delta)/4$. Here, $\mp\Delta/2$ are the energies of the d_{3y^2-1} and $d_{x^2-z^2}$ orbitals in cell 3 (Fig. 1), $-\delta/2$ is the matrix element between them, and $(\Delta^2 + \delta^2)^{1/2} \equiv Xt$ is the crystal-field splitting. We see that the e_g band is cut $\frac{3}{2}t = \frac{1}{4}W$ above the bottom and $\frac{3}{2}t$ below the top, with gaps of size Xt , so that the band *overlap* is merely $(3-X)t + \mathcal{O}(X^2)$. For the 11 and 0 GPa structures, respectively, $(\Delta, \delta) = (500, 110)$ and $(849, 126)$ meV, and $X = 0.94$ and 1.85 . For large X , the density of states (DOS) *gap* is found to be $(X-4)t + \mathcal{O}(X^{-2})$.

Inclusion of the spin and the e_g - t_{2g} repulsion in the static mean field approximation splits the e_g band by $2\mathcal{J}S$ into e_g^\uparrow and e_g^\downarrow bands with spins locally parallel and antiparallel to that of the t_{2g} spin. Because of the random orientation of the latter, the e_g hopping integrals are independent of spin and *reduced* by the factor $\frac{2}{3}$ [17]. Since the coupling between the e_g^\uparrow and e_g^\downarrow bands is of order $t'^2/2\mathcal{J}S$, the DOS gap remains $(X' - 3.6)t'$ to order t' . Here, $t' \equiv \frac{2}{3}t$, $X't' \equiv Xt$ is the crystal-field splitting, and the value 3.6 for the IM transition was obtained numerically; it lies between the small and large- X limits.

Finally, the e_{g1}^\uparrow - e_{g2}^\uparrow Coulomb repulsion, $U'' \approx U' - J = 2.75$ eV, splits the occupied and empty e_g^\uparrow bands apart by the *effective* crystal field:

$$(\Delta^2 + \delta^2)_{eff}^{1/2} \approx (\Delta^2 + \delta^2)^{1/2} + (n_1^\uparrow - n_2^\uparrow) U''. \quad (2)$$

The orbital polarization, $n_1^\uparrow - n_2^\uparrow \equiv P(X'_{eff})$, is a band-structure function which increases linearly from 0, reaches 0.8 for $X'_{eff} = 3.6$, and saturates at 1 for large X'_{eff} . As a consequence, Eq. (2) written in the form: $\frac{2}{3}X'_{eff} = X + P(X'_{eff})U''/t$ is the self-consistency condition for the effective crystal-field splitting and orbital polarization as functions of the band-structure parameters t and X . This equation explains the dashed lines in Fig. 3 and yields the band structures shown in the third line of Fig. 2. Note that, in contrast to DMFT, the LDA+ U approximation gives a spontaneous orbital polarization of the cubic band structure at normal volume.

In conclusion, the IM transition in LaMnO₃ at 32 GPa is not of Mott-Hubbard type. Rather, it is triggered by small distortions which create a crystal-field splitting, strongly enhanced by the Coulomb repulsion. For sufficiently large splitting, the majority-spin e_g bands separate and LaMnO₃ becomes an insulator. Crucial are also the bandwidth reductions of $\frac{2}{3}$ and $\frac{3.6}{6}$ arising from, respectively, the spatially uncorrelated directions of the t_{2g} spins at room temperature and the cutting by the effective crystal field of the e_g band in two subbands which

overlap by less than the bandwidth.

We acknowledge helpful discussions with O. Gunnarsson, P. Horsch, G. Khaliullin, I. Loa, and K. Syassen, as well as support by the Deutsche Forschungsgemeinschaft through the Emmy Noether program (K.H.,M.F.).

Note added in proof.— An LDA+ U study similar to ours, albeit for 0 K and 0 GPa, was reported in Ref. [19].

-
- [1] R. von Helmolt *et al.*, Phys. Rev. Lett. **71**, 2331 (1993); S. Jin *et al.*, Science **264**, 413 (1994); P. Schiffer *et al.*, Phys. Rev. Lett. **75**, 3336 (1995).
 - [2] A. E. Bocquet *et al.*, Phys. Rev. B **46**, 3771 (1992); M. Abbate *et al.*, Phys. Rev. B **46**, 4511 (1992); A. Chainani *et al.*, Phys. Rev. B **47**, 15397 (1993); T. Saitoh *et al.*, Phys. Rev. B **56**, 8836 (1997).
 - [3] J.-H. Park *et al.*, Phys. Rev. Lett. **76**, 4215 (1996).
 - [4] Y. Okimoto *et al.*, Phys. Rev. Lett. **75**, 109 (1995); K. Takenaka *et al.*, J. Phys. Soc. Jpn. **68**, 1828 (1999); K. Tobe *et al.*, Phys. Rev. B **64**, 184421(R) (2001); M. A. Quijada *et al.*, Phys. Rev. B **64**, 224426 (2001); N. N. Kovaleva *et al.*, Phys. Rev. Lett. **93**, 147204 (2004).
 - [5] I. Loa *et al.*, Phys. Rev. Lett. **87**, 125501 (2001).
 - [6] G. Banach and W. M. Temmerman, J. Phys.: Condens. Matter **16**, S5633 (2004); H. Zenia *et al.*, New J. Phys. **7**, 257 (2005).
 - [7] G. Trimarchi and N. Binggeli, Phys. Rev. B **71**, 035101 (2005).
 - [8] V. I. Anisimov *et al.*, Phys. Rev. B **44**, 943 (1991).
 - [9] V.I. Anisimov *et al.*, J. Phys.: Condens. Matter **9**, 7359 (1997); A.I. Lichtenstein and M.I. Katsnelson, Phys. Rev. B **57**, 6884 (1998); K. Held *et al.*, Psi-k Newsletter **56**, 5 (2003).
 - [10] O. K. Andersen and T. Saha-Dasgupta, Phys. Rev. B **62**, R16219 (2000); E. Zurek *et al.*, ChemPhysChem **6**, 1934 (2005).
 - [11] E. Pavarini *et al.*, New J. Phys. **7**, 188 (2005); E. Pavarini *et al.*, Phys. Rev. Lett. **92**, 176403 (2004).
 - [12] S. Satpathy *et al.*, Phys. Rev. Lett. **76**, 960 (1996); W. E. Pickett and D. J. Singh, Phys. Rev. B **53**, 1146 (1996); I. Solovyev *et al.*, Phys. Rev. Lett. **76**, 4825 (1996); Phys. Rev. B **53**, 7158 (1996); H. Sawada *et al.*, Phys. B **56**, 12154 (1997); I. S. Elfimov *et al.*, Phys. Rev. Lett. **82**, 4264 (1999).
 - [13] N. Marzari and D. Vanderbilt, Phys. Rev. B **56**, 12847 (1997).
 - [14] W. Metzner and D. Vollhardt, Phys. Rev. Lett. **62**, 324 (1989); A. Georges *et al.*, Rev. Mod. Phys. **68**, 13 (1996).
 - [15] Y. Motome and M. Imada, J. Phys. Soc. Jpn. **68**, 16 (1999); K. Held and D. Vollhardt, Phys. Rev. Lett. **84**, 5168 (2000); V. Ferrari and M. J. Rozenberg, Mod. Phys. Lett. B **15**, 1031 (2001); Th. Pruschke and M.B. Zöfl, Adv. in Solid State Phys. **40**, 251 (2001); M. S. Laad *et al.*, New J. Phys. **6**, 157 (2004).
 - [16] LDA+DMFT tests for cubic LaMnO₃ at 0 GPa and 600 K gave *no* spontaneous orbital polarization.
 - [17] K.H. Ahn and A.J. Millis, Phys. Rev. B **61**, 13545 (2000).
 - [18] G. Sangiovanni *et al.*, cond-mat/0511442.
 - [19] W.-G. Yin *et al.*, Phys. Rev. Lett. **96**, 116405 (2006).